IEEE Access
Multidisciplinary ⋮ Rapid Review ⋮ Open Access Journal

Received 21 June 2023, accepted 12 July 2023, date of publication 20 July 2023, date of current version 27 July 2023.

Digital Object Identifier 10.1109/ACCESS.2023.3297441

RESEARCH ARTICLE

Computer Aided Diagnosis for Gastrointestinal Cancer Classification Using Hybrid Rice Optimization With Deep Learning

OLFAT M. MIRZA[1], AISHA ALSOBHI[2], TAWFIQ HASANIN[2], MOHAMAD KHAIRI ISHAK[3], FATEN KHALID KARIM[4], AND SAMIH M. MOSTAFA[5,6]

[1]Department of Computer Science, College of Computers and Information Systems, Umm Al-Qura University, Makkah 24382, Saudi Arabia
[2]Department of Information Systems, Faculty of Computing and Information Technology, King Abdulaziz University, Jeddah 21589, Saudi Arabia
[3]School of Electrical and Electronic Engineering, Universiti Sains Malaysia, Engineering Campus, Nibong Tebal, Pulau Pinang 14300, Malaysia
[4]Department of Computer Sciences, College of Computer and Information Sciences, Princess Nourah bint Abdulrahman University, Riyadh 11671, Saudi Arabia
[5]Computer Science Department, Faculty of Computers and Information, South Valley University, Qena 83523, Egypt
[6]Faculty of Industry and Energy Technology, New Assiut Technological University (NATU), New Assiut City 71684, Egypt

Corresponding author: Samih M. Mostafa (samih_montser@sci.svu.edu.eg)

This work was supported by Princess Nourah bint Abdulrahman University Researchers Supporting Project number (PNURSP2023R300), Princess Nourah bint Abdulrahman University, Riyadh, Saudi Arabia.

ABSTRACT A gastrointestinal disease is a group of cancers which mainly affects the digestive system, along with the stomach, small intestine, oesophagus, rectum, and colon. Accurate classification and earlier diagnosis of this cancer are crucial for better patient outcomes. Deep learning (DL) algorithm, especially convolutional neural network (CNN), is trained to categorize endoscopic images of gastrointestinal tissue as either benign or malignant. Gastrointestinal cancer (GC) classification with DL is the process of using artificial intelligence (AI), especially the DL algorithm, to categorize endoscopic images of gastric tissue as benign or malignant. It could help clinicians to identify the earliest symptoms of cancer and make treatment decisions, resulting in improved patient outcomes. The study designs a new gastrointestinal disease Detection and Classification using Hybrid Rice Optimization with Deep Learning (GDDC-HRODL) model. The presented GDDC-HRODL model intends to classify the medical images for GC. To achieve this, the GDDC-HRODL technique initially preprocesses the input data to improve image quality. In addition, the presented GDDC-HRODL algorithm employs the HybridNet model to produce feature vectors and the hyperparameter tuning process takes place using the HRO algorithm. For GC classification purposes, the GDDC-HRODL technique uses an attention-based long short-term memory (ALSTM) model and its hyperparameters can be selected by the ant lion optimization (ALO) algorithm. The design of hyperparameter tuning processes helps to accomplish enhanced GC classification performance. The experimental analysis of the GDDC-HRODL algorithm on the medical dataset demonstrates its betterment in the GC classification process.

INDEX TERMS Artificial intelligence, gastric cancer classification, deep learning, medical imaging, hyperparameter tuning, hybrid rice optimization.

I. INTRODUCTION

Gastric cancer (GC) has commonly occurred in the cavity organs with the maximum prevalence that was a severe threat to health [1]. The diagnosis of GC is relevant to the disease phase. The treatment and diagnosis of earlier GC are useful for the recovery of patients, and the survival rate of patients is exceeded up to 90%. But it is found that many patients are in an advanced stage [2]. Owing to the inadequate treatment, the survivability of advanced GC is

The associate editor coordinating the review of this manuscript and approving it for publication was M. Venkateshkumar.

lower and the diagnosis is poor [3]. With the enhancement of people's health awareness and the progression of medical devices, the treatment and diagnosis of GC are becoming an urgent need for many victims. Thus, enhancing the precision of GC identification, particularly initial GC, has been the focus of recent studies [4]. GC can be assessed by imaging examination, endoscopy, pathological pictures, and so on. Initially, endoscopy was broadly utilized in GC detection. Image-enhanced endoscopies, like linked color imaging and narrow-band imaging, can precisely scrutinize the structure of the surface [5]. The research works stated that the implementation of such endoscopic techniques could enrich the precision of GC diagnosis. In tumor diagnostics, pathology slides were routinely set from resections or biopsies and cancer tissue was stained with hematoxylin and eosin (HE) [6].

With whole-slide scanners, histological slides are transformed into digital imageries encompassing complicated visual data that can be mined by artificial neural networks (ANN) [7]. Convolutional Neural Network (CNN) was an existing deep-learning (DL) technique that was proven effective computational mechanism for image classifications. Several difficulties should be resolved before the medical application of digital biomarkers, the DL concept might have incredible advantages for therapeutic and diagnostic decisions. Advancements of digital biomarkers in DL-based tumor pathology for typical cancer types were recently studied [8]. The emergence of whole-slide images (WSI) led to the application of medical imaging analysis methods to help pathologists in diagnosing and reviewing WSIs cancer [9], [10]. Particularly, deep CNNs (DCNN) have shown existing outcomes in medicinal imaging analysis and a large number of computer vision (CV) applications [9]. Successful and Promising computational pathology applications involve tumor segmentation and classification, resultant predictive and mutation classification. Such results emphasize the potential large advantages that could be gained while deploying DL-related tools and workflow mechanisms to support histopathological diagnosis and to help surgical pathologists, particularly for rising diagnostic double-reading and primary screening efficiency [10].

This study focuses on the development of automated gastrointestinal cancer Detection and Classification using the Hybrid Rice Optimization with Deep Learning (GDDC-HRODL) model. The presented GDDC-HRODL model primarily preprocesses the input data to improve image quality. Next, the presented GDDC-HRODL technique employs the HybridNet model to produce feature vectors and the hyperparameter tuning process takes place using the HRO algorithm. For GC classification purposes, the GDDC-HRODL technique uses an attention-based long short-term memory (ALSTM) model and its hyperparameters can be selected by the ant lion optimization (ALO) algorithm. The experimental result analysis of the GDDC-HRODL technique takes place on the medical dataset.

II. RELATED WORKS

In [11], a multi-scale visual transformer method so-called GasHis-Transformer was presented for Gastric Histopathological Image Detection (GHID) that allows the automated global recognition of GC images. The gasHis-Transformer method comprises 2 key components planned for extracting local and global data utilizing a position-encoder transformer system and CNN with local convolution correspondingly. Additionally, a Dropconnect-based lightweight network was presented for reducing the size of models and trained time of GasHis-Transformer for medical application with enhanced confidence. Wang et al. [12] present a Smart connected electronic gastroscope (SCEG), a smart-connected electronic gastroscopy scheme which carries out dynamic cancer screening from gastroscopy. The authors establish an AdaBoost-based multiple-column CNN (MCNN) to enhance GC screening by combining electronic gastroscopy with a cloud-based medicinal image diagnosis service.

Togo et al. [13] established an automated gastritis recognition scheme utilizing double-contrast upper gastrointestinal barium X-ray radiography. The researcher planned a DCNN-based GC recognition method and estimated the efficacy of the technique. The recognition efficiency of our process has been related to ABC (D) stratification. Hmoud Al-Adhaileh et al. [14] present 3 networks, AlexNet, GoogleNet, and ResNet50 that are dependent upon DL and estimate them for their potential in analyzing a database of lesser GC diseases. Every image is improved, and the noise was removed beforehand so it can be inputted into the DL network. During this classifier step, pre-trained CNN techniques are changed by transfer learning (TL) for performing novel tasks. The Softmax function takes a deep feature vector and categorizes the input images into 5 classes.

Sun et al. [15] intended to establish and validate a DL radiomics method to estimate serosa invasion from GC. Traditional hand-crafted and DL features can be removed in the 3 stages of Computed tomography (CT) images and are employed for building radiomics signatures using ML techniques. Integrating the radiomics signature and CT finding, a radiomics nomogram has been established using multivariable LR. Zhang et al. [16] designed a CT-based radiomic method for predicting advanced GC (AGC) patients effectively. Radiomic feature is extracted from the input CT images and the ML model is utilized for the classification process. Sakai et al. [17] presented a CNN-based automatic recognition system for helping the initial analysis of GC from endoscopic images. The authors executed TL utilizing 2 classes (normal and cancer) of image databases which are detailed texture data on lesions developed in a smaller count of annotated images.

III. THE PROPOSED MODEL

In this study, we have designed a novel GDDC-HRODL system for GC detection and classification. The presented GDDC-HRODL methodology exploits DL with a hyperparameter tuning process for GC classification. It follows a

series of subprocesses namely contrast enhancement, HybridNet feature extractor, HRO-based hyperparameter tuning, ALSTM classification, and ALO-based parameter tuning. Fig. 1 exhibits the working flow of the GDDC-HRODL approach.

A. CONTRAST ENHANCEMENT

The CLAHE (contrast limited adaptive histogram equalization) is a novel way of enhancing the contrast in an image. It is widely employed in medical imaging to improve the visibility of structure in an image and optimize the diagnosis quality of an image [18]. The fundamental concept behind the CLAHE is to split the images into smaller regions, named tiles, and separately employ histogram equalization to all the tiles [18]. Histogram equalization is a process which adjusts the intensity value of the pixel in the image whereby the resultant images have a uniform distribution of intensity value. The contrast limiting factor in the CLAHE prevents the intensity value from being extremely stretched, causing loss of detail and over-saturation in an image. This might assist in preserving the local structure of an image and prevent the ''washed out'' appearance that takes place with standard histogram equalization. The CLAHE algorithm is effective for an image that has a larger dynamic range or lower contrast, like medical imaging. It is used for improving the visibility of subtle features in the image, namely smaller vessels or abnormalities, and making them more obvious to the observer.

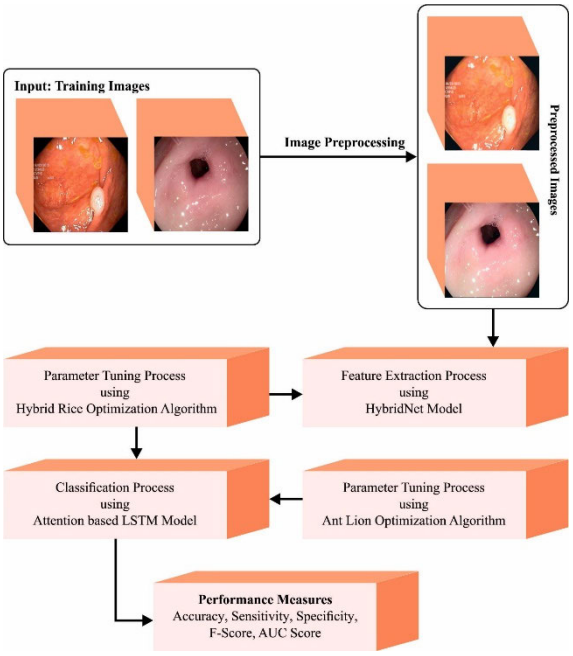

FIGURE 1. Working flow of GDDC-HRODL approach.

B. FEATURE EXTRACTION PROCESS

For the generation of feature vectors, the HybirdNet model is used. HybridNet has encompassed two Autoencoder (AE) paths, the unsupervised path (E_u and D_u) and the discriminator path (E_u and D_u) [19]. The encoders E_c and E_u take the input image x and generate representation h_c and h_u, whereas decoders D_c and D_u take correspondingly h_c and h_u as input for generating $\hat{x}_c$ and $\hat{x}_u$ partial reconstructions. Lastly, the C classifier generates a class prediction using discriminator features: $\hat{y} = C(h_c)$. Although the two paths might have the same architecture. The discrimination path extracts discriminatory features $\hat{x}_c$ that must be crafted well eventually to efficiently implement the classification tasks and generate a deliberately partial reconstruction $\hat{x}$. As a result, the unsupervised path role is to be complementary to the discriminatory branch by maintaining h_u the data missing in h_c. This technique could generate a complementary reconstruction $\hat{x}_c$ such that, while fusing $\hat{x}$ and $\hat{x}$, the ultimate reconstruction $\hat{x}$ is nearby to x.

$$\begin{aligned} h_c &= E_c(x) \quad \hat{x} = D_c(h_c) \quad \hat{y} = C(h_c) \\ h_u &= E_u(x) \quad \hat{x} = D_u(h_u) \quad \hat{x} = \hat{x}_c + \hat{x}_u \end{aligned} \tag{1}$$

It should be noted that the reconstruction model is performed as regularised for the discriminatory encoder. The major contribution and challenge of the study are to develop a method to make sure that both paths would execute in a desired manner. The two major problems that we address are the fact that the discriminator branch needs to be focused on the discriminatory feature and that both branches want to be contributed and co-operated towards the reconstruction. Using this framework, two paths are worked individually: a reconstruction path $\hat{x} = \hat{x}_u = D_u(E_u(x))$ and a classification path $\hat{y} = C(E_c(x))$ and $\hat{x}_c = 0$. Then, tackle these problems by using the structural design of the encoder and decoder along with the training procedure and appropriate loss. The HybridNet framework has two data paths with class prediction and parts that need that incorporated. The study is tackling the question of training these architectures effectively. It encompasses the term for classification with $\mathcal{L}_{cls}$; last reconstruction with $\mathcal{L}_{rec}$; intermediate reconstruction with $\mathcal{L}_{rec-interb,l}$ (for branch b and layer l); and stability with $\Omega_{stability}$. Every term can be weighted using the respective variable λ:

$$\mathcal{L} = \lambda_c \mathcal{L}_{cls} + \lambda_r \mathcal{L}_{rec} + \sum_{b\epsilon\{c,u\}} \lambda_{rb,l} \mathcal{L}_{rec-interb,l} + \lambda_s \Omega_{stability} \tag{2}$$

HybridNet is trained on the partially labelled datasets, viz., labelled pairs $\mathcal{D}_{\text{sup}} = \{(x^{(k)}, y^{(k)})\}_{k=1..N_s}$ and unlabelled images $\mathcal{D}_{unsup} = \{x^{(k)}\}_{k=1..N_u}$. All the batches are encompassed of n samples, separated into n_s image-label pair from $\mathcal{D}_{\text{sup}}$ and n_u unlabelled image from $\mathcal{D}_{unsup}$. The classification term is exploited only on n_s labelled instances of the batch and averaged over them:

$$\begin{aligned} \ell_{cls} &= \ell_{CE}(\hat{y}, y) = -\sum_i y_i \log \hat{y}_i, \mathcal{L}_{cls} \\ &= \frac{1}{n_s} \sum_k \ell_{cls}\left(\hat{y}, y^{(k)}\right) \end{aligned} \tag{3}$$

C. HYPERPARAMETER TUNING PROCESS

In this work, the hyperparameter tuning of HybirdNet architecture takes place with the use of the HRO algorithm. HRO is a metaheuristic technique which mimics the breeding method of three-line hybrid rice seeds [20]. In all the iterations, the population of rice seeds are arranged by fitness from greater to lesser and divided into three subpopulations. Based on symmetry and self-equilibrium, every subpopulation is intended as an equivalent number of individuals. The individual in the fitness level is chosen into the maintainer line, the sterile line, and the restorer line. The HRO comprises three phases: renewal, selfing, and hybridization.

1) HYBRIDIZATION

Hybridization was implemented to renew the rice seed gene in the sterile line. Two types of rice seed populations were introduced to recreate novel individuals that are chosen at random in the maintainer and sterile line, correspondingly. When the novel rice seeds are better than the existing ones, the present rice seed would be replaced with the novel one. The novel gene by hybridizing has been demonstrated as follows:

$$X_{new(i)}^{k} = \frac{r_1 X_{s,r}^{k} + r_2 X_{m,r}^{k}}{r_1 + r_2} \tag{4}$$

In Eq. (4), $X_{new(i)}^{k}$ denotes the new k^{th} genes of i^{th} rice seeds in the sterile line, $X_{s,r}^{k}$ indicates the k^{th} genes of the randomly chosen individual from the sterile line, $X_{m,r}^{k}$ represents the k^{th} genes of the randomly chosen individual from the maintainer line, r_1 and r_2 are a randomly generated number lies in $[-1, 1]$.

Selfing behavior improves the gene sequences of rice seed in the restorer line that making rice seed progressively get closer to the better one, and the equation can be updated as follows:

$$X_{new(i)} = rand\ (0, 1) \cdot \left(X_{besi} - X_{j,r}\right) + X_i \tag{5}$$

In Eq. (5), $X_{new(i)}$ denotes the newly produced individual by selfing of the i^{th} restorer, X_{best} signifies the present optimum solution and $X_{j,r}$ indicates the j^{th} randomly chosen individual from the restorer line ($i \neq j$). When the novel individuals are superior to the older individuals, then older individuals can be swapped with the current and new self-crossing number (t) which is fixed as zero, or else $t_i = t_i + 1$.

2) RENEWAL

The presented phase is a reset process for rice seed from the restorer line that hasn't been upgraded for $t_{\max}$ successive times, and the renewal approach has been demonstrated as follows:

$$X_{new(i)} = X_i + rand\ (0, 1) \cdot (R_{\max} - R_{\min}) + R_{\min} \tag{6}$$

In Eq. (6), $X_{new(i)}$ indicates the newly produced individual by the renewal of i^{th} restorer, $R_{\max}$ and $R_{\min}$ signify the maximum and minimum limitations of the search space.

For binary coding, every individual in the population can be characterized by the binary string where every component is limited only to zero or one. Every candidate solution from the rice seed should be mapped to the probability value which takes zero or one to resolve the problem of band selection. Thus, a sigmoid function is applied for achieving data transformation and is shown in the following:

$$S\ (x) = \frac{1}{1 + e^{-x}} \tag{7}$$

$$X_i^k = \begin{cases} 1, & S(X_i^k) > 0.5 \\ 0, & else \end{cases} \tag{8}$$

From the expression, x indicates the real number, and x_i^k characterizes the k^{th} genes of the i^{th} novel rice seeds.

Algorithm 1 Pseudocode of HRO Algorithm

Input: the predetermined parameter of HR
Output: the fitness function value and global optimum solution
Randomly initializing the rice seed population
Initializing $t_i = 0, k = 0$
While (k<maximal amount of iterations)
Assess the fitness function of all the rice seed
Split the rice seed into 3 lines
For all the rice seeds in the sterile line
Choose respective rice seeds randomly at the sterile and maintainer line
The novel gene can be attained using Eq. (4)
If the novel rice seeds are optimum
Upgrade the present rice seeds
End if
End for
For every rice seed at the restorer line
If $t_i < t_{\max}$
The new rice seed can be attained using Eq. (5)
If the new rice seeds are optimum
Upgrade the rice seeds
$t_j = 0$
Else
$t_j = t_j + 1$
End if
Else
The rice seeds are renewed using Eq. (6)
End if
End for
$k = k + 1$
End whil

D. GC CLASSIFICATION USING OPTIMAL ALSTM MODEL

Finally, the proposed model exploits the ALSTM model for GC classification. The LSTM is an NN-based recurrent neural network (RNN) that could efficiently address the issues of gradient exploding and vanishing seen in conventional

NNs [21]. Using the storage unit, the long-term timing data has been stored for capturing the long-term dependency. As per these features, LSTM-NN is widely used to handle time series tasks. The storage unit of LSTM-NN preserves 3 gates at every time step, involving input, forget and output gates. Because of the gating, the proposed model could recognize filtering and memory functions. The forgetting gate integrates the h^{t-1} hidden layer of the preceding time step with x^t input key features of the existing time step. With the sigmoid function, each input feature is ranged within the range of zero and one, also the scaling values are used for controlling the forgotten degree of *the* C^{t-1} cell state of the preceding time step. The forget gate is expressed in the following:

$$F_t = Sigmoid\left(\sum_{j=1}^{J} W_j^{Fx} x_j^t + \sum_{l=1}^{L} W_l^{Fh} h_l^{t-1} + b_F\right) \quad (9)$$

In Eq. (9), J and L denote the dimension of x^t input feature vectors and h^{t-1} hidden layers, correspondingly, W and b indicate the weight matrix and bias in every gate. The input gate integrates x^t and h^{t-1} for generating novel candidate value $\tilde{C}_t$ through the tanh activation function. Like forgetting gates, the scaled values are utilized for controlling the degree to which the candidate value is upgraded. The input gate can be expressed by:

$$\tilde{C}_t = tanh\left(\sum_{j=1}^{J} W_j^{\tilde{C}x} x_j^t + \sum_{l=1}^{L} W_l^{\tilde{C}h} h_l^{t-1} + b_{\tilde{c}}\right) \quad (10)$$

$$I_t = sigmoid\left(\sum_{j=1}^{J} W_j^{Ix} x_j^t + \sum_{l=1}^{L} W_l^{Ih} h_l^{t-1} + b_I\right) \quad (11)$$

Next, the existing cell state C_t is upgraded using Eq. (12):

$$C_t = F_t * C_{t-1} + I_t * \tilde{C}_t \quad (12)$$

The output gate defines which part of the data is to be transferred for the present $C_t$cell state. The output gate can be formulated by:

$$O_t = sigmoid\left(\sum_{j=1}^{J} W_j^{Ox} x_j^t + \sum_{l=1}^{L} W_l^{Oh} h_l^{t-1} + b_O\right) \quad (13)$$

$$h^t = O_t * tanh\left(C_t\right) \quad (14)$$

The primary objective of the attention module is to simulate human visual processes. For instance, once people notice something, they tend to give greater consideration towards certain data that could help judgment and disregard redundant data. The attention module could be assumed as a weighted summation that could assign respective weights as per the significance of input features. Fig. 2 showcases the architecture of ALSTM.

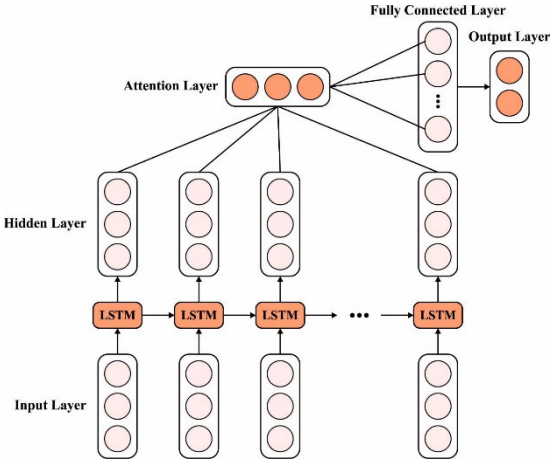

FIGURE 2. Structure of ALSTM.

The computation equation can be given in the following:

$$\alpha_m = sigmoid\left(\sum_{l=1}^{L} W_l^{\alpha h} h_l^m + b_\alpha\right) \quad (15)$$

$$\beta_m = \frac{e^{\alpha_m}}{\sum_{q=1}^{T} e^{\alpha_q}} \quad (16)$$

$$\gamma = \sum_{m=1}^{T} \beta_m h^m \quad (17)$$

Now, T indicates the overall time step; h^m shows the vector of output feature; α_m represents the results of the first weighted computation through the fully connected (FC) layer; $W_p^{\alpha h}$ and b_α represent the weight matrices and biases of the FC layer, correspondingly; β_m represent the final weight allocated to the respective h^m computed using the softmax function, and γ denote the key feature of extraction. The LSTM-NN architecture contains the input vectors $x^1, x^2, \ldots\ldots, x^t$ are key feature vectors. The LSTM architecture disposes of the input vector in the time step and attains multiple hidden layers $h^1, h^2, \ldots\ldots, h^t$. The attention model evaluates the attention weight β_m through NN with the softmax activation function. Next, the attention to weight β_m is allocated to the respective hidden layer h^m. Lastly, the key feature γ is extracted through summation. The LSTM hyperparameters can be adjusted by the use of the ALO algorithm. Seyedali Mirjalili establishes the ALO, a unique population-based stochastic search approach which stimulates ant lion hunting processes [22]. During the sand, an ant lion larva excavates a cone-shaped hole. The 5 stages of the ALO technique for hunting the prey such as catching prey, building traps, re-building traps, and entrapping prey in traps. The random walks (RW) begin after establishing primary Ant places and antlions from the searching space at random. The subsequent definition offers the mathematical equation of these walks:

$$S(t) = [0, cumsum\left(2u\left(t_1\right) - 1\right), cumsum\left(2u\left(t_2\right) - 1\right), \ldots cumsum\left(2u\left(t_{T\max}\right) - 1\right) \quad (18)$$

whereas *cumsum* defines the entire cumulative sum of consecutive random stages that include the RW up to present time t, $T_{\max}$ is the maximal iteration count and $u(t)$ denotes the stochastic function determined as in Eq. (19):

$$u(t) = \begin{cases} 1 & if\ rand > 0.5 \\ 0 & if\ rand \leq 0.5 \end{cases} \tag{19}$$

In which, *rand* implies the random number with uniform distribution generated from the range of zero and one. The RW of Ant_i nearly a given $Alion_j^t$ has normalized utilizing Eq. (20) for maintaining RW in the searching space.

$$S_i^t = \frac{(S_i^t - a_i) \times (q_i - p_i^t)}{(q_i^t - a_i)} + p_i \tag{20}$$

In which q_i^t refers to the maximal RW of i^{th} Ant at the t^{th} iteration, p_i^t signifies the minimal RW of i^{th} Ant at the t^{th} iteration that refers to the dynamic boundary neighboring the Alion, and a_i implies the minimal RW of i^{th} Ant. It is mathematically determined in Eq. (21).

$$\begin{aligned} p_i^t &= Alion\ jt + p^t \\ q_i^t &= Alion\ jt + q^t \end{aligned} \tag{21}$$

If the Ant falls into the pit, it attempts to exit. The radius of Ant's RW has decreased adaptively by utilizing Eq. (22) for modelling this performance mathematically.

$$\begin{aligned} p^t &= \frac{p^t}{I} \\ q^t &= \frac{q^t}{I} \end{aligned} \tag{22}$$

whereas I denote the sliding ratio parameter which monitors the exploitation or exploration rates and is determined in Eq. (23):

$$I = 10^g \frac{t}{T_{\max}} \tag{23}$$

whereas g refers to the constant demonstrating the present iteration $T_{\max}$ signifies the iteration counts, ($g = 2$ if $t > 0.1T_{\max}$, $g = 3$ if $t > 0.5T_{\max}$, $g = 4$ if $t > 0.75T_{\max}$, $g = 5$ if $t > 0.9T_{\max}$, and $g = 6$ if $t > 0.95T_{\max}$). The constant g is employed for adjusting the count of exploitation accuracy. Prey is assumed that caught once an ant takes more suitable than their equivalent antlion. For improving their capability for hunting novel ants, the antlion needs to change their place to that of caught ants. Eq. (24) defines this operation:

$$Alion_j^t = \begin{cases} a_i^t & if\ f(Ant_i^t) < f(Alion_j^t) \\ Alion_j^t & otherwise \end{cases} \tag{24}$$

To do all the iterations, the Alion with maximal fitness was allocated eliteAlion. The chosen process is then utilized, whereas "Alion" was altered to "Ant" when the "Ant" gains additional fitness. Eq. (25) was utilized for updating the ant position.

$$Ant_i^t = \frac{W_A^t + W_E^t}{2} \tag{25}$$

W_E^t refers to the representation of chosen processes RW nearby the chosen Alion. The ALO system is a higher possibility of solving local better stagnation as it creates utilization of RWs and roulette wheel. The ALO technique's random choice of ant lions, random movement of ants in their environment, and adaptive reduction bounds on ant lions' traps make sure the exploitation of searching spaces. The ALO is demonstrated in the subsequent procedure (l), per the above-mentioned formula. The ALO algorithm derives a fitness function to conquer better efficiency of the classification and determine the positive integer to describe the superior performance of candidate results. Here, the decline of the classifier rate of errors can be regarded as a fitness function, as follows.

$$\begin{aligned} fitness\,(x_i) &= Classifier\ Error\ Rate\,(x_i) \\ &= \frac{number\ of\ misclassified\ samples}{Tota\ lnumber\ of\ samples} * 100 \end{aligned} \tag{26}$$

IV. RESULTS AND DISCUSSION

In this section, the experimental validation of the GDDC-HRODL approach is tested using the Kvasir dataset [23]. Table 1 gives details on the dataset. It comprises of interpret images by experts, containing classes including endoscopic processes from the gastrointestinal tract and anatomical landmarks. The database comprises 5000 images which are enough for utilization in DL and TL. The database is in RGB colour space and comprises images from resolution in 720 × 576 up to 1920 × 1072 pixels. During this work, the database comprises 5 diseases normal pylorus, ulcerative colitis, dyed-lifted polyps, normal cecum, and polyps. Fig. 3 represents the sample images.

TABLE 1. Details of the dataset.

Labels	Class	No. of Samples
C-1	Dyed-Lifted Polyps	1000
C-2	Normal-Cecum	1000
C-3	Normal-Pylorus	1000
C-4	Polyps	1000
C-5	Ulcerative Colitis	1000
Total No. of Samples		5000

The confusion matrix attained by the GDDC-HRODL model during the execution process is illustrated in Fig. 4. The outcomes demonstrate that the GDDC-HRODL approach has properly categorized all five class labels.

In Table 2 and Fig. 5, the overall classifier outcomes of the GDDC-HRODL approach are briefly provided. The results show that the GDDC-HRODL model obtains effectual

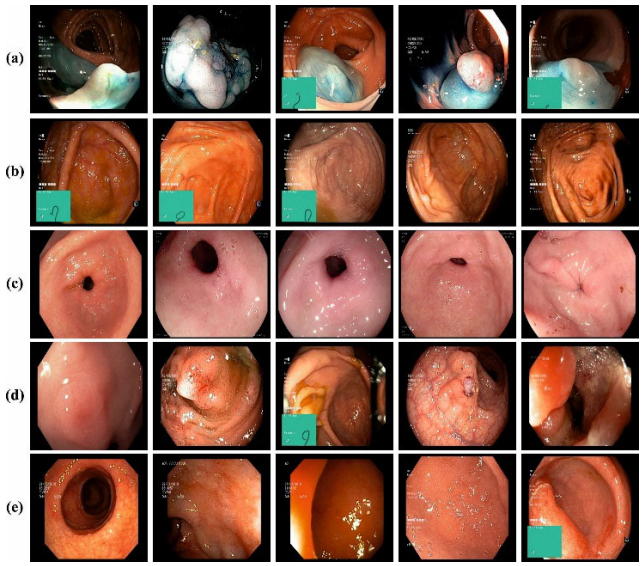

a) Dyed-Lifted Polyps b) Normal-Cecum c) Normal-Pylorus d) Pylorus e) Ulcerative Colitis

FIGURE 3. Sample images.

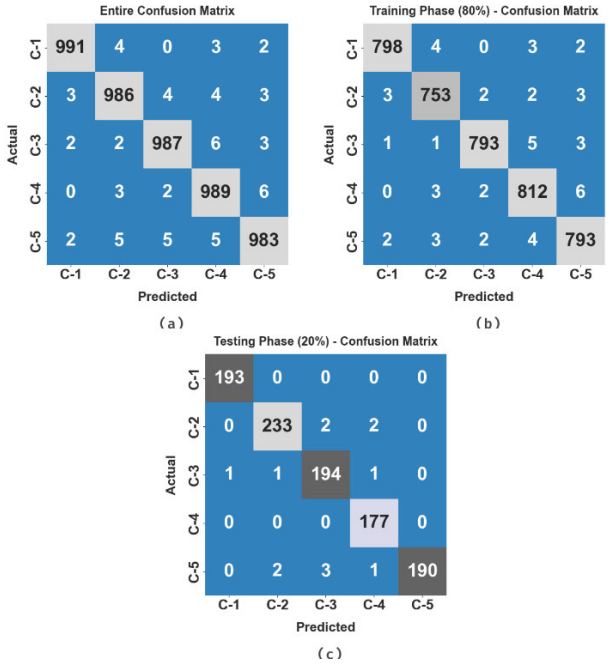

FIGURE 4. Confusion matrices of GDDC-HRODL system (a) Entire database, (b) TRS of 80% and (c) TSS of 20%.

TABLE 2. Classifier outcome of GDDC-HRODL system with distinct classes and measures.

Labels	Accuracy	Sensitivity	Specificity	F-Score	AUC Score
Entire Dataset					
C-1	99.68	99.10	99.82	99.20	99.46
C-2	99.44	98.60	99.65	98.60	99.12
C-3	99.52	98.70	99.72	98.80	99.21
C-4	99.42	98.90	99.55	98.56	99.23
C-5	99.38	98.30	99.65	98.45	98.98
Average	99.49	98.72	99.68	98.72	99.20
Training Phase (80%)					
C-1	99.62	98.88	99.81	99.07	99.35
C-2	99.48	98.69	99.66	98.62	99.17
C-3	99.60	98.75	99.81	99.00	99.28
C-4	99.38	98.66	99.56	98.48	99.11
C-5	99.38	98.63	99.56	98.45	99.10
Average	99.49	98.72	99.68	98.73	99.20
Testing Phase (20%)					
C-1	99.90	100.00	99.88	99.74	99.94
C-2	99.30	98.31	99.61	98.52	98.96
C-3	99.20	98.48	99.38	97.98	98.93
C-4	99.60	100.00	99.51	98.88	99.76
C-5	99.40	96.94	100.00	98.45	98.47
Average	99.48	98.75	99.67	98.71	99.21

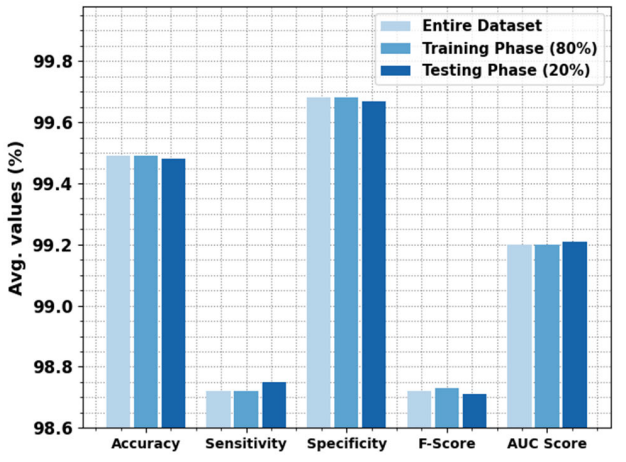

FIGURE 5. Average outcome of GDDC-HRODL system with distinct zmeasures.

outcomes under each class. On the entire dataset, the GDDC-HRODL model obtains an average $accu_y$ of 99.49%, $sens_y$ of 98.72%, $spec_y$ of 99.68%, F_{score} of 98.72%, and AUC_{score} of 99.20%. Similarly, on 80% of the training set (TRS), the GDDC-HRODL approach gains an average $accu_y$ of 99.49%, $sens_y$ of 98.72%, $spec_y$ of 99.68%, F_{score} of 98.73%, and AUC_{score} of 99.20%. Likewise, on 20% of the testing set (TSS), the GDDC-HRODL technique attains an average $accu_y$ of 99.48%, $sens_y$ of 98.75%, $spec_y$ of 99.67%, F_{score} of 98.71%, and AUC_{score} of 99.21%.

The training $accu_y$ (TACY) and validation $accu_y$ VACY of the GDDC-HRODL algorithm are investigated on gastrointestinal disease detection performance in Fig. 6. The figure pointed out that the GDDC-HRODL method has exposed higher performance with maximal values of TACY and VACY. The GDDC-HRODL technique has gained maximal TACY outcomes.

The training loss (TLOS) and validation loss (VLOS) of the GDDC-HRODL methodology are tested on gastrointestinal disease detection performance in Fig. 7. The figure specified

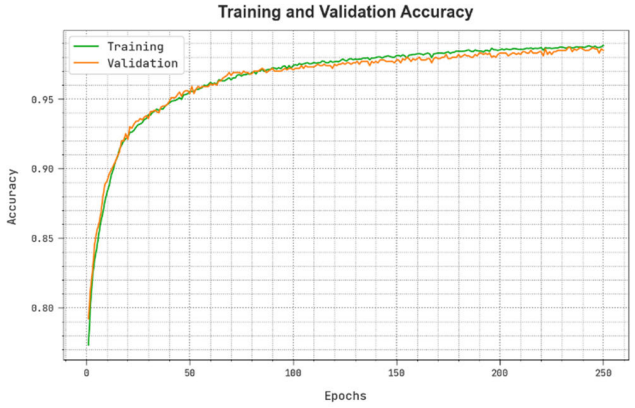

FIGURE 6. TACY and VACY outcome of GDDC-HRODL system.

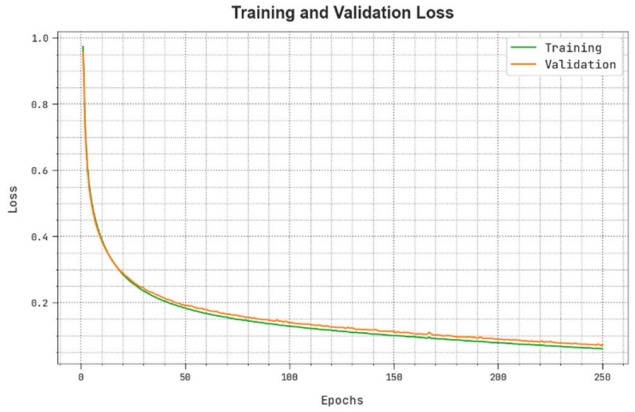

FIGURE 7. TLOS and VLOS outcome of GDDC-HRODL system.

that the GDDC-HRODL algorithm has revealed optimum performance with lesser values of TLOS and VLOS. It is noticed that the GDDC-HRODL system has resulted in lesser VLOS outcomes.

An evident precision-recall study of the GDDC-HRODL approach in the test database is displayed in Fig. 8. The figure implied that the GDDC-HRODL system has led to maximum values of precision-recall values in distinct five classes.

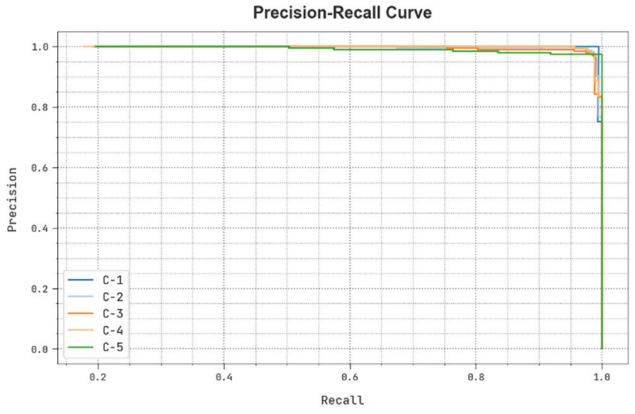

FIGURE 8. Precision-recall outcome of GDDC-HRODL system.

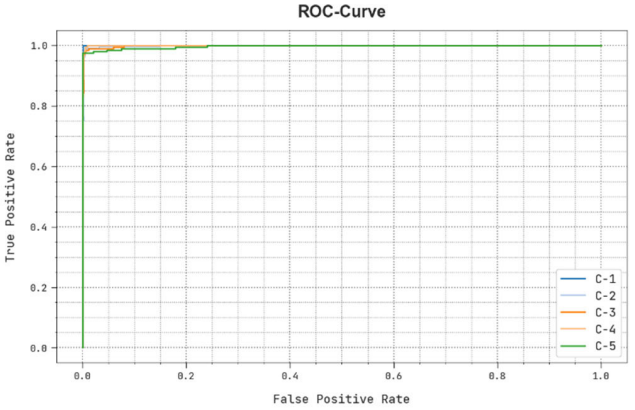

FIGURE 9. ROC outcome of GDDC-HRODL system.

TABLE 3. Comparative outcome of GDDC-HRODL approach with recent DL systems.

Methods	Accuracy	Sensitivity	Specificity	AUC	CT (s)
GDDC-HRODL	99.49	98.72	99.68	99.20	2.67
DL Model	97.35	96.74	97.03	98.69	3.89
Augmented CNN	99.00	98.68	97.70	96.05	3.16
AlexNet	96.43	97.64	99.01	98.59	4.23
GoogleNet	98.76	96.60	98.92	97.02	4.19
ResNet-50	97.77	96.73	99.10	96.90	3.92

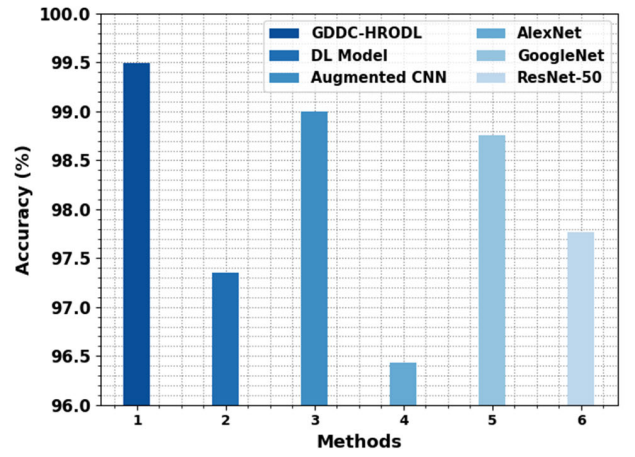

FIGURE 10. Comparative outcome of GDDC-HRODL approach with recent DL systems.

A comprehensive ROC study of the GDDC-HRODL system in the test database is shown in Fig. 9. The outcomes exposed the GDDC-HRODL methodology has revealed its capability in categorizing five several classes.

The experimental outcomes of the GDDC-HRODL technique are compared with recent DL approaches in Table 3 and Fig. 10 [14], [24], [25]. The obtained values indicated that the AlexNet model reaches poor performance with the least $accu_y$ of 96.43%, $sens_y$ of 97.64%, $spec_y$ of 99.01%,

and AUC of 98.59%. In addition, it is noticed that the DL and ResNet-50 models obtain closer classification results with $accu_y$ of 97.35% and 97.77% respectively.

At the same time, the augmented CNN model manages to portray reasonable performance with $anaccu_y$ of 99%, $sens_y$ of 98.68%, $spec_y$ of 97.70%, and AUC of 96.05%. However, the GDDC-HRODL model gains maximum performance with $anaccu_y$ of 99.49%, $sens_y$ of 98.72%, $spec_y$ of 99.68%, and AUC of 99.20%. Furthermore, the proposed model reaches a minimal CT value over other models. These results highlighted the superior performance of the GDDC-HRODL technique over recent DL methods.

V. CONCLUSION

In this study, we have designed a novel GDDC-HRODL system for GC detection and classifier. The projected GDDC-HRODL model primarily preprocessed the input data to improve image quality. Next, the presented GDDC-HRODL technique employs the HybridNet model to produce feature vectors and the hyperparameter tuning process takes place using the HRO algorithm. For GC classification purposes, the GDDC-HRODL technique uses the ALSTM model and its hyperparameters can be selected by the ALO algorithm. The experimental result investigation of the GDDC-HRODL system occurs on the medical dataset. The comparative result analysis pointed out the better performance of the GDDC-HRODL technique over other models. In future, the performance of the proposed approach is improvised by the ensemble learning process.

ACKNOWLEDGMENT

Princess Nourah bint Abdulrahman University Researchers Supporting Project number (PNURSP2023R300), Princess Nourah bint Abdulrahman University, Riyadh, Saudi Arabia.

REFERENCES

[1] Y. Zhao, B. Hu, Y. Wang, X. Yin, Y. Jiang, and X. Zhu, "Identification of gastric cancer with convolutional neural networks: A systematic review," *Multimedia Tools Appl.*, vol. 81, no. 8, pp. 11717–11736, 2022.

[2] S. Kuntz, E. Krieghoff-Henning, J. N. Kather, T. Jutzi, J. Höhn, L. Kiehl, A. Hekler, E. Alwers, C. von Kalle, S. Fröhling, J. S. Utikal, H. Brenner, M. Hoffmeister, and T. J. Brinker, "Gastrointestinal cancer classification and prognostication from histology using deep learning: Systematic review," *Eur. J. Cancer*, vol. 155, pp. 200–215, Sep. 2021.

[3] L.-S. Li, X.-Y. Guo, and K. Sun, "Recent advances in blood-based and artificial intelligence-enhanced approaches for gastrointestinal cancer diagnosis," *World J. Gastroenterol.*, vol. 27, no. 34, pp. 5666–5681, Sep. 2021.

[4] C. Li, Y. Qin, W. Zhang, H. Jiang, B. Song, M. R. Bashir, H. Xu, T. Duan, M. Fang, L. Zhong, L. Meng, D. Dong, Z. Hu, J. Tian, and J.-K. Hu, "Deep learning-based AI model for signet-ring cell carcinoma diagnosis and chemotherapy response prediction in gastric cancer," *Med. Phys.*, vol. 49, no. 3, pp. 1535–1546, Mar. 2022.

[5] P. Podder, S. Bharati, and M. R. H. Mondal, "10 automated gastric cancer detection and classification using machine learning," in *Artificial Intelligence for Data-Driven Medical Diagnosis*. Berlin, Germany: De Gruyter, 2021, pp. 207–224.

[6] X. Zheng et al., "A deep learning model and human-machine fusion for prediction of EBV-associated gastric cancer from histopathology," *Nature Commun.*, vol. 13, no. 1, pp. 1–12, May 2022.

[7] P.-C. Chen, Y.-R. Lu, Y.-N. Kang, and C.-C. Chang, "The accuracy of artificial intelligence in the endoscopic diagnosis of early gastric cancer: Pooled analysis study," *J. Med. Internet Res.*, vol. 24, no. 5, May 2022, Art. no. e27694.

[8] P.-H. Niu, L.-L. Zhao, H.-L. Wu, D.-B. Zhao, and Y.-T. Chen, "Artificial intelligence in gastric cancer: Application and future perspectives," *World J. Gastroenterol.*, vol. 26, no. 36, pp. 5408–5419, Sep. 2020.

[9] Z. Xiao, D. Ji, F. Li, Z. Li, and Z. Bao, "Application of artificial intelligence in early gastric cancer diagnosis," *Digestion*, vol. 103, no. 1, pp. 69–75, 2022.

[10] H. Hu, L. Gong, D. Dong, L. Zhu, M. Wang, J. He, L. Shu, Y. Cai, S. Cai, W. Su, Y. Zhong, C. Li, Y. Zhu, M. Fang, L. Zhong, X. Yang, P. Zhou, and J. Tian, "Identifying early gastric cancer under magnifying narrow-band images with deep learning: A multicenter study," *Gastrointestinal Endoscopy*, vol. 93, no. 6, pp. 1333–1341, Jun. 2021.

[11] H. Chen, C. Li, G. Wang, X. Li, M. M. Rahaman, H. Sun, W. Hu, Y. Li, W. Liu, C. Sun, S. Ai, and M. Grzegorzek, "GasHis-Transformer: A multi-scale visual transformer approach for gastric histopathological image detection," *Pattern Recognit.*, vol. 130, Oct. 2022, Art. no. 108827.

[12] H. Wang, S. Ding, D. Wu, Y. Zhang, and S. Yang, "Smart connected electronic gastroscope system for gastric cancer screening using multi-column convolutional neural networks," *Int. J. Prod. Res.*, vol. 57, no. 21, pp. 6795–6806, Nov. 2019.

[13] R. Togo, N. Yamamichi, K. Mabe, Y. Takahashi, C. Takeuchi, M. Kato, N. Sakamoto, K. Ishihara, T. Ogawa, and M. Haseyama, "Detection of gastritis by a deep convolutional neural network from double-contrast upper gastrointestinal barium X-ray radiography," *J. Gastroenterol.*, vol. 54, no. 4, pp. 321–329, Apr. 2019.

[14] M. H. Al-Adhaileh, E. M. Senan, F. W. Alsaade, T. H. H. Aldhyani, N. Alsharif, A. A. Alqarni, M. I. Uddin, M. Y. Alzahrani, E. D. Alzain, and M. E. Jadhav, "Deep learning algorithms for detection and classification of gastrointestinal diseases," *Complexity*, vol. 2021, Oct. 2021, Art. no. 6170416.

[15] R.-J. Sun, M.-J. Fang, L. Tang, X.-T. Li, Q.-Y. Lu, D. Dong, J. Tian, and Y.-S. Sun, "CT-based deep learning radiomics analysis for evaluation of serosa invasion in advanced gastric cancer," *Eur. J. Radiol.*, vol. 132, Nov. 2020, Art. no. 109277.

[16] W. Zhang, M. Fang, D. Dong, X. Wang, X. Ke, L. Zhang, C. Hu, L. Guo, X. Guan, J. Zhou, X. Shan, and J. Tian, "Development and validation of a CT-based radiomic nomogram for preoperative prediction of early recurrence in advanced gastric cancer," *Radiotherapy Oncol.*, vol. 145, pp. 13–20, Apr. 2020.

[17] Y. Sakai, S. Takemoto, K. Hori, M. Nishimura, H. Ikematsu, T. Yano, and H. Yokota, "Automatic detection of early gastric cancer in endoscopic images using a transferring convolutional neural network," in *Proc. 40th Annu. Int. Conf. IEEE Eng. Med. Biol. Soc. (EMBC)*, Jul. 2018, pp. 4138–4141.

[18] A. M. Reza, "Realization of the contrast limited adaptive histogram equalization (CLAHE) for real-time image enhancement," *J. VLSI Signal Process.-Syst. Signal, Image, Video Technol.*, vol. 38, no. 1, pp. 35–44, Aug. 2004.

[19] T. Robert, N. Thome, and M. Cord, "HybridNet: Classification and reconstruction cooperation for semi-supervised learning," in *Proc. Eur. Conf. Comput. Vis. (ECCV)*, Oct. 2018, pp. 153–169.

[20] Z. Shu, Z. Ye, X. Zong, S. Liu, D. Zhang, C. Wang, and M. Wang, "A modified hybrid rice optimization algorithm for solving 0–1 knapsack problem," *Appl. Intell.*, vol. 52, no. 5, pp. 5751–5769, Mar. 2022.

[21] M. Visa and D. Patel, "Attention based long-short term memory model for product recommendations with multiple timesteps," in *Proc. 5th Int. Conf. Comput. Methodol. Commun. (ICCMC)*, Apr. 2021, pp. 605–612.

[22] S. Saman and S. J. Narayanan, "An improved ant-lion optimization for deep and handcrafted feature selection in MR brain tumor classification," *Evol. Intell.*, doi: 10.21203/rs.3.rs-2308867/v1.

[23] *Kvasir: A Multi-Class Image-Dataset for Computer Aided Gastrointestinal Disease Detection*. Accessed: Mar. 20, 2023. [Online]. Available: https://datasets.simula.no/kvasir/#download

[24] A. M. Godkhindi and R. M. Gowda, "Automated detection of polyps in CT colonography images using deep learning algorithms in colon cancer diagnosis," in *Proc. Int. Conf. Energy, Commun., Data Anal. Soft Comput. (ICECDS)*, Chennai, India, Aug. 2017, pp. 1722–1728.

[25] R. Fonollá, F. van der Sommen, R. M. Schreuder, E. J. Schoon, and P. H. de With, "Multi-modal classification of polyp malignancy using CNN features with balanced class augmentation," in *Proc. IEEE 16th Int. Symp. Biomed. Imag. (ISBI)*, Venice, Italy, Apr. 2019, pp. 74–78.